Analysis of metastasis-related risk factors and clinical relevance in adult soft-tissue sarcoma

SHUAI HAN[1*], XIN SONG[1*], JIALIANG LIU[2*], JINGFEN ZHOU[1], ZHIPENG WU[2], HAIHAN SONG[3], JUN TAO[4] and JIAN WANG[1]

[1]Department of Orthopedics, Shanghai Pudong New Area People's Hospital, Shanghai 201299, P.R. China; [2]Department of Orthopedic Oncology, Shanghai Changzheng Hospital, Naval Medical University, Shanghai 200003, P.R. China; [3]Central Laboratory of Shanghai Key Laboratory of Pathogenic Fungi Medical Testing, Shanghai Pudong New Area People's Hospital, Shanghai 201299, P.R. China; [4]Department of Orthopedics, Weihai Central Hospital, Qingdao University, Shandong 264499, P.R. China

Received March 29, 2024; Accepted July 19, 2024

DOI: 10.3892/ol.2024.14647

Abstract. Metastasis occurs in nearly 50% of cases of adult soft-tissue sarcoma (ASTS), leading to a dismal prognosis, with a 2-year survival rate of ~30%. Consequently, a prognostic model that incorporates metastatic characteristics may be instrumental in predicting survival time and in crafting optimal personalized therapeutic strategies for patients with ASTS. In the present study, a prognostic prediction model for ASTS was developed by examining genes that are differentially expressed between non-metastatic and metastatic patients in the Gene Expression Omnibus dataset. The prognostic model, which includes five featured genes [actin γ2 (ACTG2), apolipoprotein D, coatomer protein complex subunit γ2 imprinted transcript 1, collagen type VI α6 chain and osteomodulin], was further validated in patients with ASTS from the Cancer Genome Atlas dataset. Based on these five-gene signatures, patients were categorized into high- and low-risk groups. Functional and pathway analyses revealed disparities in stemness, extracellular matrix and cell adhesion-related pathways between the two risk groups, particularly noting the activation of the PI3K-Akt pathway in high-risk cases. Analysis of immune infiltration also revealed variations in immune microenvironment changes between the two risk groups. Immunohistochemical staining substantiated the prognostic significance of these gene signatures in a specific sarcoma subtype. Additionally, wound-healing and Transwell assays demonstrated that inhibition of ACTG2 by shRNAs curbed cell migration and invasion in a sarcoma HOS cell line, underscoring its role in sarcoma metastasis. In conclusion, the present study successfully developed and validated a metastasis-based prognosis prediction model. This model not only reliably forecasts the survival of patients with ASTS, but also may pave the way for further investigation into the processes underlying sarcoma metastasis, ultimately aiding in the design of tailored therapeutic regimens.

Correspondence to: Professor Jian Wang, Department of Orthopedics, Shanghai Pudong New Area People's Hospital, 490 Chuanhuan South Road, Chuansha, Pudong New Area, Shanghai 201299, P.R. China
E-mail: wjwj0328@163.com

Professor Jun Tao, Department of Orthopedics, Weihai Central Hospital, Qingdao University, 3 West Mishan Road, Wendeng, Weihai, Shandong 264499, P.R. China
E-mail: tjspine@gmail.com

*Contributed equally

Key words: adult soft-tissue sarcoma, metastasis, prognostic signature, immune infiltration, ACTG2

Introduction

Adult soft-tissue sarcoma (ASTS) encompasses a wide array of rare solid tumors, stemming from mesenchymal tissue, with ~175 distinct subtypes (1). Epidemiologically, ASTS accounts for merely 1% of all human malignancies (2), with >13,000 new cases identified in the United States as per the 2019 Cancer Statistics report (3). Recently, advancements have been made in treatments for ASTS, including surgical resection, chemotherapy, targeted therapy, immunotherapy and radiotherapy (3,4). Despite these advancements, the overall survival (OS) prognosis for patients with ASTS remains poor, with a 5-year survival rate of ~65% (5), largely due to the high risk of local recurrence and metastasis.

Metastasis is a predominant cause of mortality among patients with ASTS, affecting 40-50% within 5 years of diagnosis (3). Patients with metastatic disease have a median survival rate of 12-16 months, with a 2-year survival rate of just 30% (6). Lung metastases are the most common, yet the precise molecular processes that drive metastasis are still not well understood (3). While clinical data can predict outcomes to some extent, its predictive accuracy is constrained by complex tumor regulatory factors. In the era of genetics, several studies have endeavored to develop prognostic prediction models focusing on specific gene functions, such as immune- or hypoxia-related genes (6,7). The adverse effects of metastasis on the prognosis of ASTS necessitates the early detection of metastatic indicators and the creation of a new

prognostic model using reliable markers with unbiased gene selection, which could enhance our understanding of ASTS progression and lead to more effective, personalized treatment strategies.

The objective of the present study was to develop and validate a prognostic model [including actin γ2 (ACTG2), apolipoprotein D (APOD), coatomer protein complex subunit γ2 imprinted transcript 1 (COPG2IT1), collagen type VI α6 chain (COL6A6) and osteomodulin (OMD)] by comparing and analyzing differentially expressed genes (DEGs) between metastatic and non-metastatic ASTS cases, utilizing online databases, and to explore the implications of this model in clinical samples. Additionally, preliminary investigations were conducted into the function of ACTG2 in a sarcoma cell line.

Materials and methods

Data collection and processing. The mRNA expression profiles of patients with ASTS were sourced from the Gene Expression Omnibus (GEO) (https://www.ncbi.nlm.nih.gov/geo/query/acc.cgi?acc=GSE21050) dataset initially created by Chibon *et al* (8), encompassing 310 sarcoma tissue samples (accession no. GSE21050). These samples were categorized into a metastasis group (n=122) and a non-metastasis group (n=188). Only patients with complete information on survival and metastasis were included in the analysis. The mRNA expression profiles comprised 54,613 entries, from which DEGs were identified using the DESeq (https://cran.r-project.org/web/packages/DESeq2/index.html) and Limma (https://cran.r-project.org/web/packages/limma/index.html) R packages. DEGs in metastatic ASTS samples, compared with non-metastatic samples, met stringent criteria, including an adjusted P-value of <0.05 and an absolute log2-based fold-change (FC) value of >1. Additionally, an external validation cohort of ASTS samples was obtained from The Cancer Genome Atlas (TCGA) database (https://portal.gdc.cancer.gov), which included 260 cases. Clinical profiles and survival information for these datasets were downloaded simultaneously.

Establishment of the gene prediction model. Following the established protocol, univariate, least absolute shrinkage and selection operator (LASSO), and multivariate Cox regression analyses were utilized to examine the correlation between OS and gene expression levels in patients.

Initially, the prognostic significance of each differentially expressed gene (DEG) was assessed using univariate Cox regression analysis facilitated by the survival R package (https://cran.r-project.org/web/packages/survival/index.html). Genes achieving P<0.1 in this analysis were deemed significant. Next, the significant prognostic genes for metastatic ASTS were narrowed down using LASSO-penalized Cox regression. This involved subsampling the dataset 1,000 times and selecting genes that appeared in >900 of these samples. The tuning parameters for LASSO were determined based on the Akaike Information Criterion (AIC) (9) using an estimation of the expected generalization error from 10-fold cross-validation, and the highest λ-value was selected. Subsequently, multivariate Cox regression analysis was conducted to evaluate the contribution of each gene as an independent prognostic factor for OS. Next, a forest map and a heatmap were generated to visually represent these contributing genes. Finally, a prognostic risk score was established for each patient using a linear combination of the gene expression levels weighted by their respective regression coefficients (β) from the multivariate Cox regression analysis. The optimal cut-off for the risk score was determined using the median value rule, which allowed us to categorize patients into low- and high-risk groups, and construct Kaplan-Meier (KM) survival curves for these groups.

Five genes identified as independent variables in the multivariate Cox regression analysis were used to create a nomogram to predict the annual OS probability for patients with ASTS. Additionally, the receiver operating characteristic (ROC) curve was plotted to evaluate the discrimination accuracy of the nomogram and a calibration plot was used to assess its predictive accuracy, using rms R software. (https://cran.r-project.org/web/packages/rms/index.html).

Functional enrichment analysis of DEGs. DEGs were identified between the high- and low-risk subgroups using specific criteria (adjusted P<0.05 and absolute log2-based FC>1). The clusterProfiler (https://cran.r-project.org/web/packages/clusterProfiler/index.html), ggplot2 (https://cran.r-project.org/web/packages/ggplot2/index.html) and enrichplot packages (https://cran.r-project.org/web/packages/enrichplot/index.html) were employed to conduct Gene Ontology (GO) and Kyoto Encyclopedia of Genes and Genomes (KEGG) analyses based on these DEGs. The GO analysis was segmented into three categories: Biological process (BP), cellular component (CC) and molecular function (MF).

Immunocyte infiltration analysis. The RNA-sequencing expression profiles and associated clinical information for patients with ASTS (key word 'Sarcoma') were obtained from TCGA dataset (https://portal.gdc.com). The proportions of the 10 types of immune cells in the high- and low-risk subgroups were estimated using the TIMER2.0 algorithm, following the official manual available on the TIMER2.0 website (http://timer.cistrome.org/). The ggstatsplot package in R (https://github.com/IndrajeetPatil/ggstatsplot) was utilized to establish the degree of correlation between gene expression and immune score, while the pheatmap package in R (https://cran.r-project.org/web/packages/pheatmap/index.html) was used to identify correlations among multiple genes. Spearman's correlation analysis was conducted to assess the correlation between quantitative variables that were not normally distributed. P<0.05 was considered to indicate a statistically significant difference.

IHC staining of the sarcoma samples. To explore the clinical relevance of these predictive genes in a specific sarcoma subtype, 90 osteosarcoma samples were collected from patients who had undergone surgical resection at Shanghai Changzheng Hospital (Shanghai, China) and Shanghai Pudong New Area People's Hospital (Shanghai, China) between January 2017 and December 2020. The follow-up data was obtained through outpatient service and telephone consultation. Patients who were lost to follow-up were excluded. The mean age of the patients was 32.2±20.2 years (range, 7-81 years), and the cohort included 49 males and 41 females.

This research was reviewed and approved by the Medical Ethics Committees of Shanghai Pudong New Area People's Hospital (no. K82 of 2021) and Shanghai Changzheng Hospital (approval no. 2018SL004), and written informed consent was obtained from all participants or their legal guardians.

The samples were fixed in 4% paraformaldehyde at room temperature for 6-12 h, sequentially dehydrated through a graded ethanol series, embedded in paraffin and sectioned into 5-μm slices. Immunohistochemical (IHC) staining for ACTG2 (cat. no. ab231802; dilution, 1:200; Abcam), APOD (cat. no. ab108191; dilution, 1:200; Abcam), COL6A6 (cat. no. HPA045239; dilution, 1:200; MilliporeSigma) and OMD (cat. no. ab154249; dilution, 1:200; Abcam) was performed (incubated at 4˚C overnight) following the standard histological procedures outlined in the Histostain-Plus (DAB) kit manual (Invitrogen; Thermo Fisher Scientific, Inc.). Goat anti-rabbit antibody (cat. no. ab205718; dilution, 1:5,000; Abcam) was used as the secondary antibody (incubated at room temperature for 1 h). Given that COPG2IT1 is a non-protein coding RNA, IHC staining was not applicable for this gene. The IHC staining results were independently evaluated by three blinded observers based on the sample characteristics. Staining intensity was rated on a scale from 0 (negative) to 3 (strongly positive), and positivity was quantified in four increments: 0 (<5%), 1 (5-25%), 2 (>25-50%), 3 (>50-75%) and 4 (>75%). The final staining score, used to classify expression as either low (score ≤4) or high (score ≥5), was calculated by multiplying the intensity by the positivity rate.

Cell line and transfection. The human HOS cell line was sourced from the Cell Bank of the China Center for Type Culture Collection of the Chinese Academy of Sciences. Cells were maintained in Dulbecco's modified Eagle's medium (DMEM) (Gibco; Thermo Fisher Scientific, Inc.) supplemented with 10% fetal bovine serum (FBS) (Gibco; Thermo Fisher Scientific, Inc.). Prior to experimentation, cells underwent mycoplasma testing. Two short hairpin (sh)RNA sequences targeting ACTG2 were obtained from Genomeditech; Jiman Biotechnology (Shanghai) Co., Ltd. The target site of sh-ACTG2#1 was 5'-GAGAGAAATTGTGCGAGACAT-3', and the target site of sh-ACTG2#2 was 5'-GCAGGTTATCAC CATTGGCAA-3'. pGenesil-1 plasmid (Shanghai Genechem Co., Ltd.) with non-mammalian targeted sequence was used as the control of sh-ACTG2. Transfection of HOS cells was performed for 24 h at 37˚C using Lipofectamine®2000 (Invitrogen; Thermo Fisher Scientific, Inc.). shRNA plasmids (5 μg) mixed with transfection reagent (10 μl) were added to each well of a 6-well plate, according to the manufacturer's protocol. The cells were then used for subsequent experiments from 24 h post-transfection.

Reverse transcription quantitative (RT-q)PCR assay. Total RNA from transfected HOS cells was extracted using TRIzol® (Thermo Fisher Scientific, Inc.) and reverse-transcribed into cDNA using Prime Script™ RT Master Mix (Takara Bio Inc.), performed at 37˚C for 30 min followed by incubation for 5 sec at 85˚C to inactivate the reverse transcriptase, according to the manufacturer's protocol. The forward primer of ACTG2 was 5'-GCGTGTAGCACCTGAAGAG-3' and the reverse primer was 5'-GAATGGCGACGTACATGGCA-3'. GAPDH was used as the loading control, with the forward primer of 5'-GGAGTCCACTGGCGTCTTCA-3' and the reverse primer of 5'-GGGGTGCTAAGCAGTTGGTG-3'. For qPCR, all reactions were performed with a hot-start preincubation step of 5 min at 95˚C, followed by 40 cycles of 25 sec at 95˚C, 30 sec at 58˚C and 20 sec at 72˚C, and a final 5 min step at 72˚C using SYBR-Green qPCR Master Mix (Selleck Chemicals) on a 7900HT Fast Real-Time PCR system (Thermo Fisher Scientific, Inc.). Expression levels were calculated using GAPDH as an internal control with the $2^{-\Delta\Delta Cq}$ method (10).

Western blot analysis. Cells were harvested with radioimmunoprecipitation assay lysis buffer at 0˚C for 30 min to obtain total proteins. Proteins were quantified using a BCA Protein Assay kit (cat. no. P0012S; Beyotime Institute of Biotechnology), and then 20 μg protein/lane was separated on 10% gels using SDS-PAGE before transfer to 0.22-mm nitrocellulose membranes. The nitrocellulose membranes were blocked using 1% BSA for 20 min at 37˚C. Subsequent to washing with TBS for 10 min at room temperature three times, the membranes were incubated overnight at 4˚C with primary antibodies against ACTG2 (1:1,000; cat. no. AF5351; Affinity Biosciences, Ltd.) and β-actin (1:1,000; cat. no. AF7018; Affinity Biosciences, Ltd.). The membranes were washed with TBS for 5 min at room temperature three times. Proteins were detected through incubation of the membranes with HRP-conjugated goat anti-rabbit IgG secondary antibody (1:5,000; cat. no. ab205718; Abcam) at 37˚C for 2 h.

Cell counting Kit-8 (CCK-8) assay. Transfected HOS cells at a seeding density of $5x10^3$ were distributed in 96-well plates and incubated for 48 h before being analyzed using the CCK-8 Kit (Selleck Chemicals). Incubation with CCK-8 was for 2 h. Absorbance was measured at 450 nm using an ELx800 microplate reader (BioTek Instruments, Inc.).

Wound-healing assay. Transfected HOS cells were cultured in 12-well plates. Once cell density reached ≥90%, the cell monolayer was scored with a 200-μl pipette tip to create a scratch, and then cultured with 2% FBS for 48 h. Wound healing was monitored by phase contrast microscopy and quantified by measuring the wound distance.

Transwell assay. An 8-μm pore size Transwell chamber precoated with Matrigel (cat. no. 354480) when purchased (Corning, Inc.) was employed to assess transfected HOC cell invasion. Chambers were seeded with $1x10^5$ cells in 100 μl serum-free DMEM, while the lower chamber was filled with 500 μl DMEM enriched with 10% FBS to serve as a chemoattractant. After incubation at 37˚C for 24 h, cells that had invaded the lower membrane surface were fixed with 4% paraformaldehyde for 20 min at room temperature, stained with 0.1% crystal violet for 30 min at room temperature, and then counted under a light microscope at x400 magnification.

Statistical analysis. Statistical analyses were performed using SPSS software (version 21.0; IBM Corp.) and R language software (https://www.r-project.org/; version R-4.0.3). Data are presented as the mean ± standard deviation. Survival curves were generated using the KM method, and the log-rank

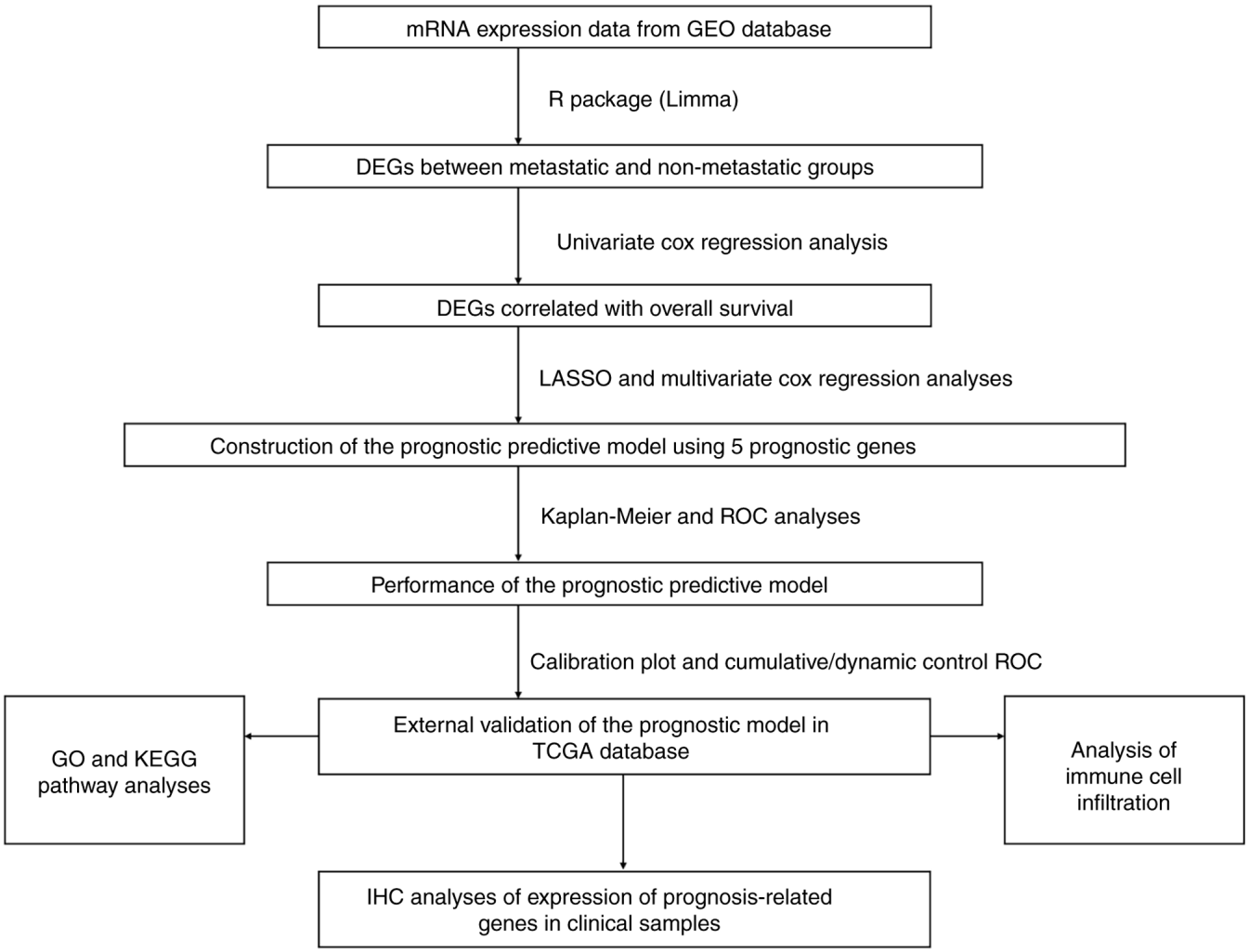

Figure 1. Workflow of the study. GEO, Gene Expression Omnibus; DEG, differentially expressed gene; LASSO, least absolute shrinkage and selection operator; ROC, receiver operating characteristic; GO, Gene Ontology; KEGG, Kyoto Encyclopedia of Genes and Genomes; TCGA, The Cancer Genome Atlas; IHC, immunohistochemistry.

test (pooled over strata) was used to analyze differences in survival between patient groups. Comparisons of qPCR, CCK8, wound-healing and Transwell assays were conducted using the one-way ANOVA analysis followed by Dunnett's (for data with unequal variances) or Fisher's least significant difference post hoc tests (for data with equal variances). $P<0.05$ was considered to indicate a statistically significant difference. All experimental procedures were repeated at least three times.

Results

Establishment of the prognosis prediction model for patients with ASTS based on metastatic gene features. The present study followed the procedural flow chart depicted in Fig. 1. DEGs between metastatic and non-metastatic ASTS samples from the GEO dataset (GSE21050) were identified using the DESeq and Limma R packages (Fig. 2A). The univariate Cox regression model was employed to pinpoint DEGs significantly associated with the OS of patients with ASTS. Following variable selection by LASSO regression, five critical genes were identified: ACTG2, APOD, COPG2IT1, COL6A6 and OMD (Fig. 2B and C). KM curves illustrated the significant correlation between the presence of these genes and the OS of patients with ASTS (Fig. 2D). Using multivariate Cox regression analysis, a regression model was formulated (Fig. 2E), and a prognostic risk score was calculated for further analysis: Risk score=ACTG2 exp. x 0.10297 + APOD exp. x (-0.1223) + COPG2IT1 exp. x (-0.23284) + COL6A6 exp. x (-0.16208) + OMD exp. x (-0.13717). The Cox coefficients and hazard ratios are detailed in Table I. Only the P-value for COL6A6 was >0.05, while the remaining results were significant.

Performance of the prognosis prediction model. Utilizing the median rule for risk scoring, patients were categorized into high- and low-risk groups (Fig. 3A). Patients in the high-risk group exhibited a higher mortality rate and shorter survival time compared with those in the low-risk group (Fig. 3B). The expression patterns of the five genes in both groups are illustrated in the form of a heatmap in Fig. 3C. The KM curve further confirmed that the high-risk group experienced significantly shorter OS times than the low-risk group (Fig. 3D). The ROC curve for the risk score in predicting survival is depicted in Fig. 3E, demonstrating an area under the curve (AUC) of 0.791.

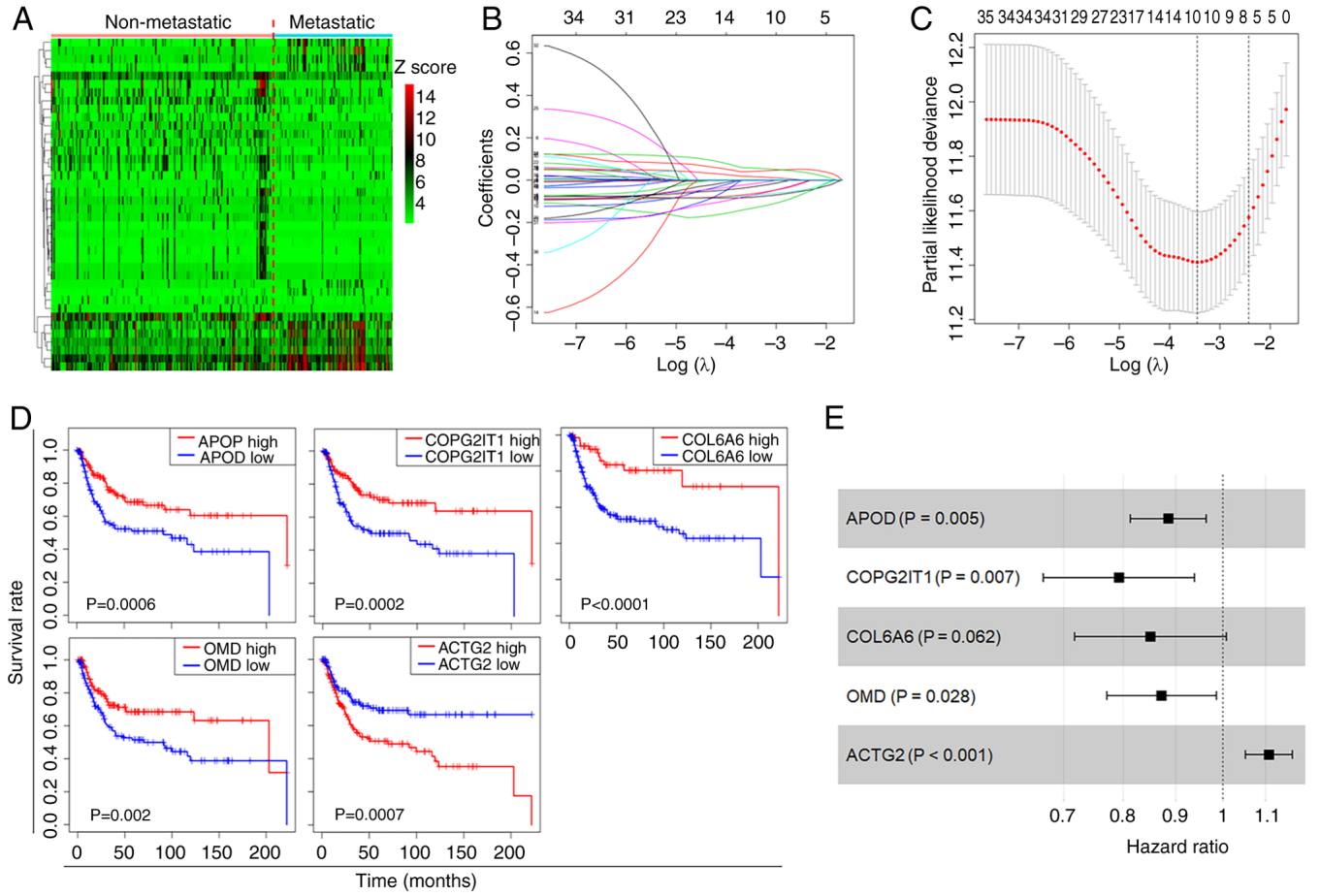

Figure 2. Construction of the metastasis-based prognosis prediction model for patients with ASTS. (A) Heatmap displaying a comparison of differentially expressed genes between metastatic and non-metastatic ASTS cases. (B) LASSO coefficient profiles of the data related to OS. (C) Selection of the tuning parameter (λ) in the LASSO model via 10-fold cross-validation based on the minimum criteria for OS. (D) Kaplan-Meier survival curves for the genes included in the prognosis prediction model. (E) Forest plot of hazard ratios from multivariate analysis of the five prognostic genes. ACTG2, actin γ2; APOD, apolipoprotein D; COPG2IT1, coatomer protein complex subunit γ2 imprinted transcript 1; COL6A6, collagen type VI α6 chain; OMD, osteomodulin; LASSO, least absolute shrinkage and selection operator; ASTS, adult soft-tissue sarcoma; OS, overall survival.

To project the annual survival rates of patients with ASTS, a nomogram was developed based on this metastasis-driven prognosis prediction model (Fig. 3F). Calibration plots showed excellent agreement between the predicted outcomes of the nomogram and actual clinical results (Fig. 3G). ROC analysis was employed to determine the sensitivity and specificity of the nomogram, with the AUC values being 0.757 at 1 year, 0.776 at 2 years, 0.786 at 3 years, 0.800 at 4 years and 0.775 at 5 years (Fig. 3H). These findings underscore the exceptional predictive capability of the risk score.

External validation of the metastatic-based prognosis prediction model in TCGA dataset. To verify the robustness of the prognosis prediction model, RNA-Seq data along with processed survival information for patients with ASTS were obtained from TCGA database. A cohort of 260 patients was classified into high- or low-risk groups using the median value derived from the same formula used in the GEO database (Fig. 4A). The high-risk group exhibited higher mortality rates and shorter survival durations compared to the low-risk group (Fig. 4B). The distribution of the expression levels of the five genes in the prognosis prediction model in both groups is depicted in the form of a heatmap in Fig. 4C. The KM curves further illustrate that the high-risk group in TCGA validation set had significantly lower OS times than the low-risk group (Fig. 4D). ROC analysis was conducted to evaluate the predictive accuracy of the nomogram system from the GEO database for the annual survival rates. In TCGA validation cohort, the AUC values on the ROC curve were 0.660 at 1 year, 0.666 at 2 years, 0.627 at 3 years, 0.618 at 4 years and 0.593 at 5 years (Fig. 4E).

Functional analysis between high- and low-risk groups. To delve into the biological functions and pathways associated with the risk model, DEGs that varied between the two risk groups were identified in both the GEO and TCGA datasets, followed by GO and KEGG analyses of these DEGs. The BP component of the GO analysis revealed significant alterations in development-related pathways between the two risk groups in both the GEO (Fig. 5A) and TCGA (Fig. S1A) datasets, indicating increased tumor cell stemness in high-risk cases (11). The CC and MF components of the GO analysis identified significant changes in collagen, extracellular matrix (ECM) and actin binding pathways between the groups in the GEO (Fig. 5B and C) and TCGA (Fig. S1B and C) datasets. These pathways are closely linked to tumor cell migration

Table I. Multivariate Cox regression analysis of genes for overall survival.

Gene	Coef	HR	95% CI	P-value
ACTG2	0.103	1.1085	1.0517-1.1682	0.0001
APOD	-0.1223	0.8849	0.8128-0.9634	0.0048
COPG2IT1	-0.2328	0.7923	0.6689-0.9385	0.0070
COL6A6	-0.1621	0.8504	0.7174-1.0079	0.0617
OMD	-0.1372	0.8718	0.7711-0.9857	0.0285

ACTG2, actin γ2; APOD, apolipoprotein D; COPG2IT1, coatomer protein complex subunit γ2 imprinted transcript 1; COL6A6, collagen type VI α6 chain; OMD, osteomodulin; Coef, coefficient; HR, hazard ratio; CI, confidence interval.

and metastasis (12,13), suggesting modifications in the tumor microenvironment during ASTS metastasis (12,14). KEGG pathway analysis indicated the activation of several migration-related pathways in high-risk cases, such as 'focal adhesion' and 'ECM-receptor interaction' pathways, across both GEO (Fig. 5D) and TCGA (Fig. S1D) datasets. Additionally, activation of the 'PI3K-Akt signaling pathway' was observed in the high-risk group, highlighting the potential of targeted therapy that addresses the PI3K-Akt pathway in high-risk patients.

Immune infiltration based on risk signature. The immune microenvironment is crucial in the pathology of tumors (15). Immune checkpoint therapies are increasingly applied in the clinical management of several types of sarcoma (16,17). Therefore, the present study analyzed the infiltration of immune cells in the two risk groups of ASTS, and assessed the correlations between the expression of the five genes from the prognosis prediction model and the infiltration of the six primary types of immune cells. The results showed that OMD and APOD were positively correlated with the presence of macrophages (r>0.3). COPG2IT1 was negatively correlated with $CD4^+$ T cell infiltration (r<-0.3), while upregulation of ACTG2 significantly predicted reduced infiltrations of dendritic cell, neutrophil and macrophages (r<-0.3) (Fig. 6A). Subsequently, the association between the risk score and 10 subtypes of immune cells was explored. The analysis revealed a significant negative correlation between the risk score and infiltration of B cells and $CD4^+$ T cells, and a positive correlation with dendritic cell (DC) infiltration (Fig. 6B). These observations imply that substantially different alterations tend to occur within the immune microenvironments of the two ASTS risk groups.

Verification of protein expression levels of the prognosis-related genes in the clinical samples. To confirm the clinical relevance of the aforementioned metastasis-based prognosis prediction model for a specific sarcoma subtype, 90 osteosarcoma samples were collected and IHC staining was conducted for the genes included in this model. Given that COPG2IT1 is a non-protein coding RNA, IHC staining was performed using antibodies specific to ACTG2, APOD, COL6A6 and OMD (Fig. 7A). The associations between the expression levels of these genes and both OS and progression-free survival (PFS) in patients were then examined. The analysis showed that the expression levels of ACTG2, APOD, COL6A6 and OMD were all significantly associated with patient OS (Fig. 7B). Moreover, the expression levels of ACTG2, APOD and OMD, but not COL6A6, were significantly associated with PFS (Fig. 7C). High expression of ACTG2 was associated with worse survival, while low expression of the other genes was associated with worse survival. This was also the case for PFS.

To assess whether combining the expression data of multiple genes could improve prognostic performance, the high expression of ACTG2 and the low expression of either APOD, COL6A6 or OMD were categorized as altered gene profiles. KM analysis revealed that combinations of multiple altered genes provided a clearer differentiation in OS and PFS compared with single genes. The combination of four altered genes yielded the lowest P-values for OS (Fig. 7D), while the combination of two altered genes achieved the lowest P-values for PFS (Fig. 7E). These findings suggest that utilizing multiple genes in the prognosis prediction model enhances the predictive accuracy for both OS and PFS in clinical samples.

Inhibition of ACTG2 suppresses cell migration and invasion, but not proliferation in a sarcoma cell line. ACTG2 was identified as the sole factor with high expression associated with a poor prognosis in this prognosis prediction model for ASTS. Consequently, the role of ACTG2 was investigated in the sarcoma HOS cell line. The effectiveness of two shRNAs for targeting ACTG2 was confirmed through RT-qPCR and western blot assays (Fig. 8A and B). Although the CCK-8 assay indicated that ACTG2 inhibition slightly reduced the proliferation rate of HOS cells compared with the control, the change was not statistically significant (Fig. 8C). However, the wound-healing assay demonstrated that ACTG2 inhibition significantly curtailed the migration of HOS cells compared with the control (Fig. 8D). Further validation using the Transwell assay showed that sh-ACTG2 markedly inhibited the invasive capabilities of the cells (Fig. 8E), indicating that ACTG2 may act as an enhancer of sarcoma metastasis.

Discussion

ASTS represents one of the most lethal malignant tumors due to its high level of heterogeneity. Additionally, with an incidence rate of ~5 cases per 100,000 individuals annually, accurately predicting its prognosis is extremely challenging (1). Despite advancements in novel therapies and combinations of chemotherapy, metastasis still occurs in nearly one-half of patients with ASTS (3). Once metastasis is present, the survival of patients with ASTS is severely jeopardized, with only a 30% 2-year survival rate (6). Consequently, identifying metastasis-related genes and constructing a survival prediction model could improve prognostic predictions for patients with ASTS during clinical treatments. In the present study, a prognosis prediction model using five gene signatures was developed by analyzing the DEGs between patients with metastatic and non-metastatic ASTS from the GEO database, and then verified in an independent series of patients with

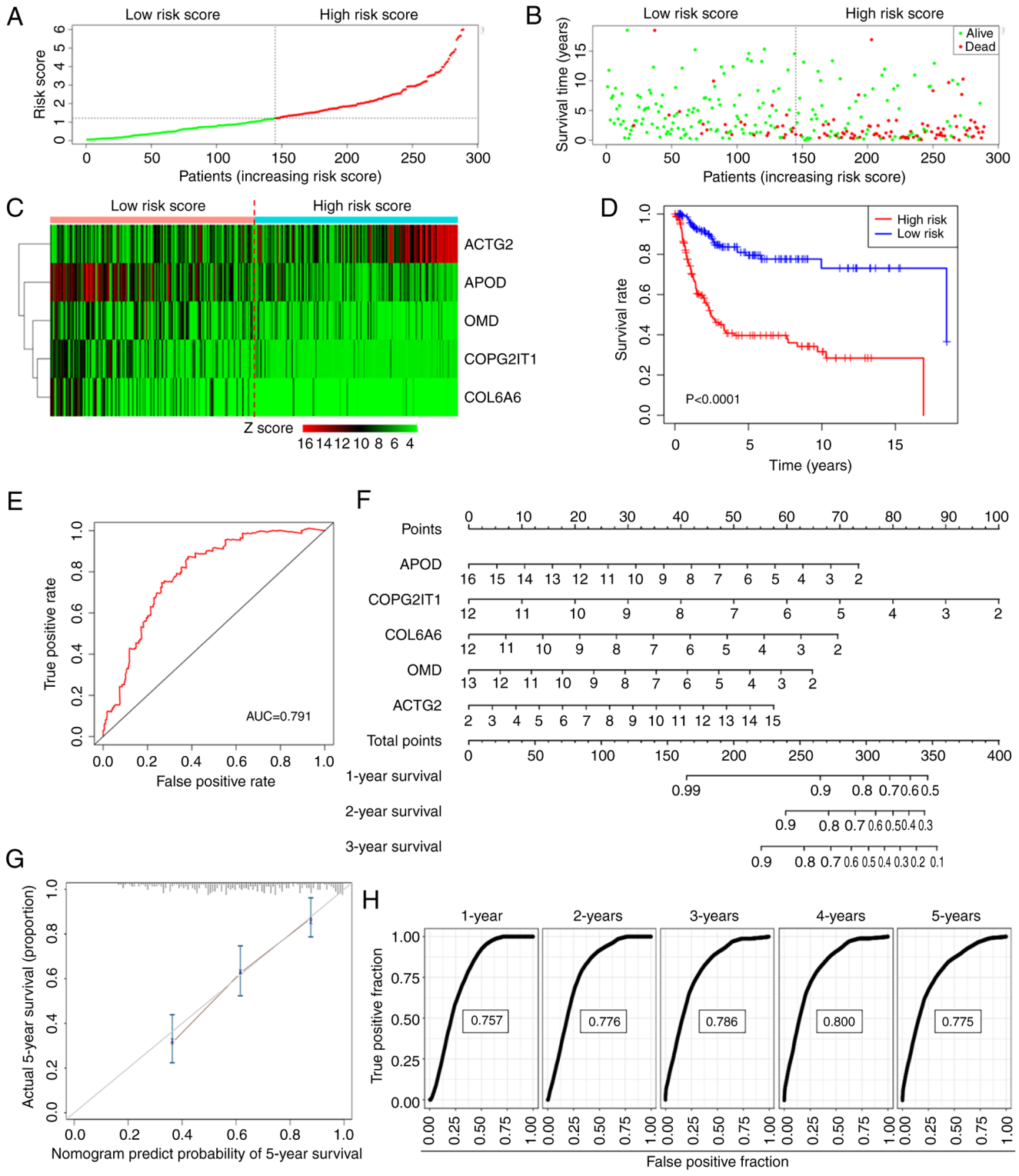

Figure 3. Assessment of the prognosis prediction model. (A) Distribution of patients categorized by risk score. (B) Distribution of survival rates associated with risk scores. (C) Heatmap of expression levels for the five prognostic genes stratified by risk score. (D) Kaplan-Meier survival curves for patients grouped according to the two risk score categories. (E) ROC curves for predicting OS using the five-gene signature. (F) A nomogram to estimate the annual survival rate of patients with adult soft-tissue sarcoma based on the five gene indicators. (G) Calibration plot for the nomogram-predicted probability of 5-year OS. (H) AUC of time-dependent ROC curves. ACTG2, actin γ2; APOD, apolipoprotein D; COPG2IT1, coatomer protein complex subunit γ2 imprinted transcript 1; COL6A6, collagen type VI α6 chain; OMD, osteomodulin; ROC, receiver operating characteristic; OS, overall survival; AUC, area under the curve.

ASTS from TCGA database. GO and KEGG analyses were performed to explore the prognosis prediction model data. The correlation between the gene signature and immunocyte infiltration was also assessed. Finally, the expression levels of genes in the prognosis prediction model were examined in a single subtype of sarcoma by IHC staining, aiming to explore the possible application of the prognostic model in clinical samples.

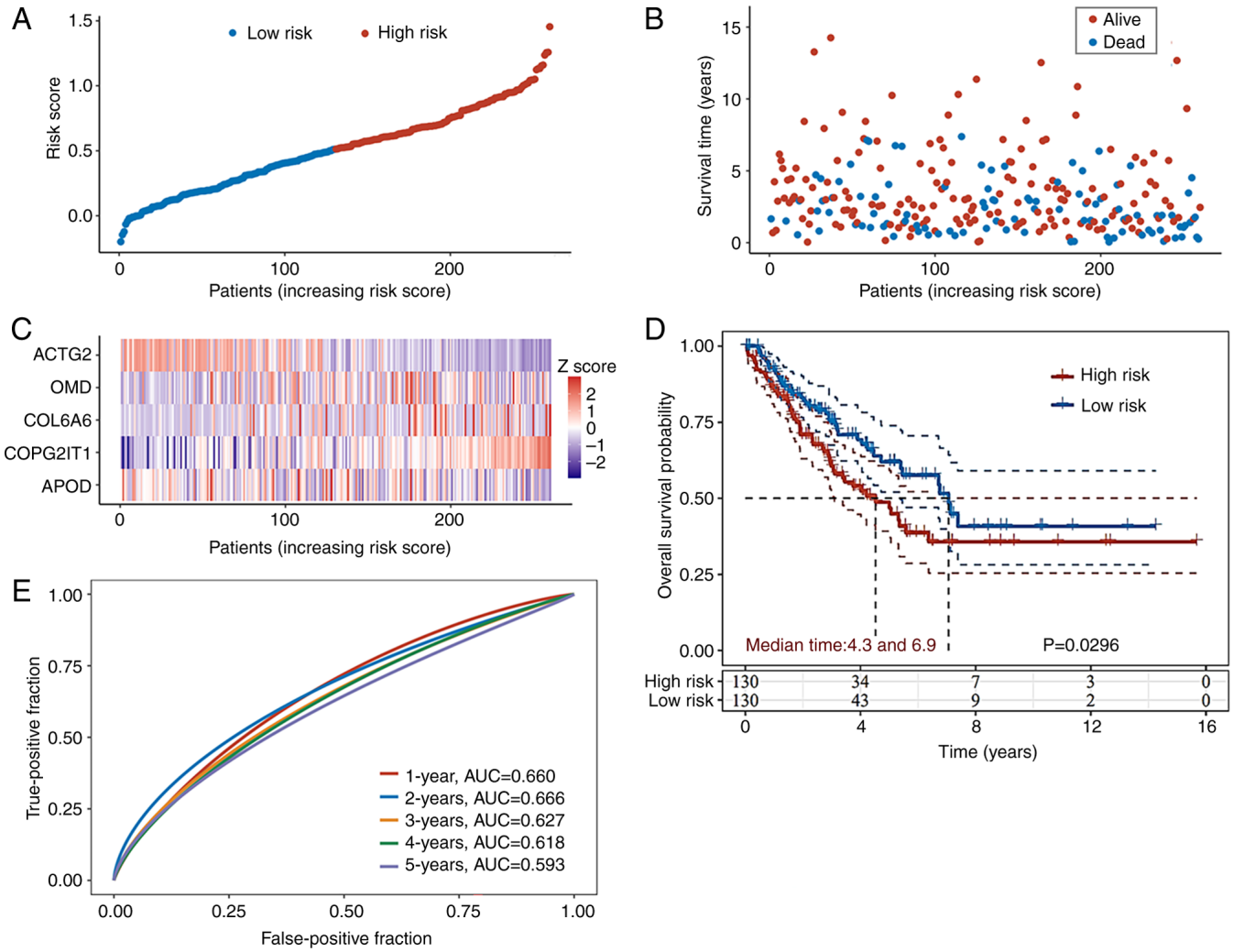

Figure 4. External validation of the prognostic model using TCGA dataset. (A) Distribution of risk scores in TCGA dataset using the five metastasis-related genes from the prognosis prediction model. (B) Survival status of patients with adult soft-tissue sarcoma in TCGA dataset categorized into high- and low-risk score groups. (C) Heatmap showing expression levels of the five prognostic genes stratified by risk score. (D) Kaplan-Meier survival curves for patients divided into the two risk score groups. (E) Receiver operating characteristic curves for predicting overall survival over a period of 1 to 5 years based on the five-gene signature. ACTG2, actin γ2; APOD, apolipoprotein D; COPG2IT1, coatomer protein complex subunit γ2 imprinted transcript 1; COL6A6, collagen type VI α6 chain; OMD, osteomodulin; TCGA, The Cancer Genome Atlas.

The prognosis prediction model comprised five genes: ACTG2, APOD, COPG2IT1, COL6A6 and OMD. The P-value of COL6A6 was 0.062 in the multivariate Cox regression model. The model selection was primarily based on the principle of minimizing the AIC. Following this AIC principle, in a multifactorial model, it is possible to include variables with P>0.05, without necessarily requiring them to be independent predictive factors (P<0.05). Thus, COL6A6 was included in the final model.

ACTG2 encodes a smooth muscle actin primarily found in the gastrointestinal system, and is linked with chronic intestinal pseudo-obstruction (18) and early onset colorectal cancer (19). Although the role of ACTG2 in other cancer types remains uncertain, Tang *et al* (20) indicated that it acts as a tumor suppressor in colorectal cancer by curtailing tumor cell proliferation. Conversely, ACTG2 has been identified as an oncogene that enhances hepatocellular carcinoma cell migration and metastasis by activating the NOTCH1 pathway (21). The ACTG2-ALK receptor tyrosine kinase fusion gene, has been implicated in the tumorigenesis and drug resistance of leiomyosarcoma, which is a subtype of ASTS (22). Additionally, ACTG2 expression has been associated with the prognosis of patients with leiomyosarcoma (23). However, the role of ACTG2 in sarcomas has rarely been explored. Therefore, the present study investigated the potential role of ACTG2 in a sarcoma cell line. The findings revealed that while inhibition of ACTG2 had a minimal effect on cell proliferation, it significantly curtailed cell migration and invasion, thus marking ACTG2 as a promoter of metastasis in ASTS.

The role of APOD in tumors remains under debate. Jankovic-Karasoulos *et al* (24) showed that elevated APOD expression facilitated breast cancer metastasis and indicated a poor prognosis. Aligning with the positive association found between APOD expression and OS in the present study, other research has noted that high APOD expression is associated with improved survival outcomes in cervical cancer (25), thyroid cancer (26) and dermatofibrosarcoma (27).

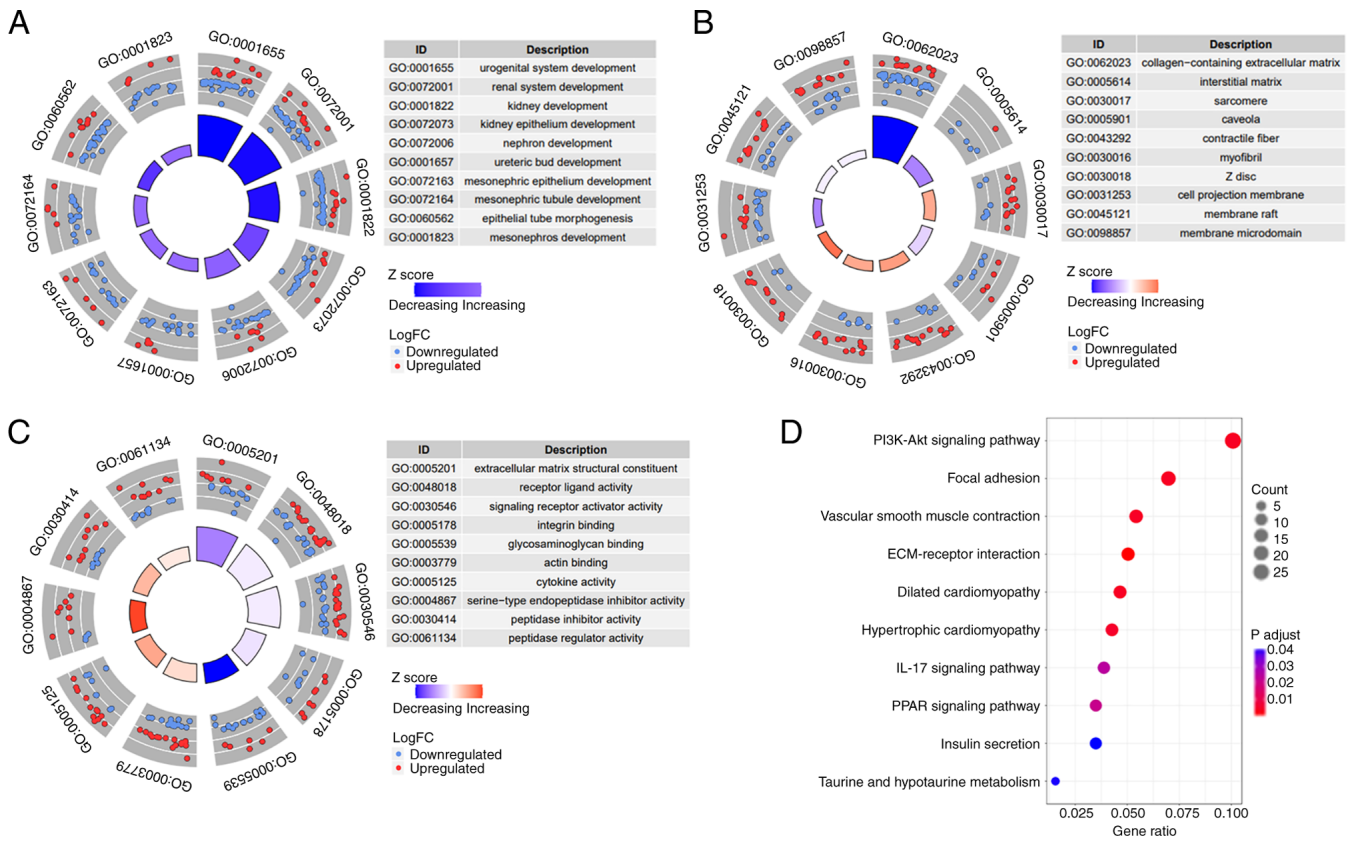

Figure 5. Functional and pathway analyses comparing the two risk groups in the Gene Expression Omnibus dataset. (A) Biological processes determined by GO analysis comparing the two risk groups. (B) Cellular components determined by GO analysis. (C) Molecular functions determined by GO analysis. (D) Kyoto Encyclopedia of Genes and Genomes pathway analysis comparing the two risk groups. FC, fold-change; GO, Gene Ontology.

COPG2IT1 belongs to the lncRNA class, but its role in sarcomas remains unclear. Green *et al* (28) demonstrated that COPG2IT1 interference occurs in infant neurobehavioral development. Mai *et al* (29) reported that COPG2IT1 was expressed at low levels in undifferentiated cells during the differentiation process of embryonic stem cells, suggesting that low expression of COPG2IT1 may contribute to the stemness of tumor cells.

COL6A6 is part of the collagen protein family, playing a role in the composition of the ECM (30). COL6A6 has been shown to inhibit tumor growth and metastasis via the JAK or PI3K-Akt pathways in non-small cell lung cancer and pituitary adenoma (31,32). Additionally, high COL6A6 expression has been identified as a favorable prognostic factor and is positively associated with the infiltration of B cells, T cells, neutrophils and DCs in lung adenocarcinoma (33). The present findings also indicated a positive correlation between COL6A6 expression and the infiltration of B cells and DCs in ASTS. Therefore, despite a P-value of 0.062 in the final model, COL6A6 was considered a key gene indicator in the prognostic model.

OMD is a small leucine-rich keratan sulfate proteoglycan found in the ECM of mineralized tissues such as bones and teeth, typically expressed by osteoblasts (34). OMD expression increases with osteoblast differentiation and supports osteoblast viability (35). In bladder cancer, OMD has been observed to suppress cancer progression by reversing epithelial-mesenchymal transition and activating cell-cell adhesion through the inhibition of the transforming growth factor-β and epidermal growth factor pathways (36). The present study also demonstrated that high OMD expression impedes tumor progression and is associated with the increased survival of patients with ASTS. Although each of the five genes has been identified to play a role in cancer, few studies have explored their potential interactions, indicating that more research is necessary.

Based on the prognosis prediction model developed in the present study, patients with ASTS were classified into high- and low-risk groups. Significant differences in OS were observed between these groups. Consequently, GO and KEGG analyses were conducted to investigate the molecular processes underlying these differences. The consistency of results across the GEO and TCGA databases confirmed the reliability of the prognosis prediction model. GO analysis indicated significant disparities in development-related pathways between the two risk groups, suggesting increased tumor cell stemness in the high-risk group, which is a critical factor in tumorigenesis, tumor progression and the drug resistance of tumors (37,38). This high stemness likely contributes to the poor prognosis observed in high-risk patients. Additionally, differences in collagen, ECM, actin binding and focal adhesion pathways, which are linked to cell-cell adhesion, were noted between the groups. Reduced cell adhesion is a crucial driver of metastasis, fostering the formation of circulating tumor cells (39) and enhancing tumor cell invasion (40). Furthermore, the ECM modulates the functions of adjacent cells through cell surface receptors, influencing tumor cell behavior (41) and immune

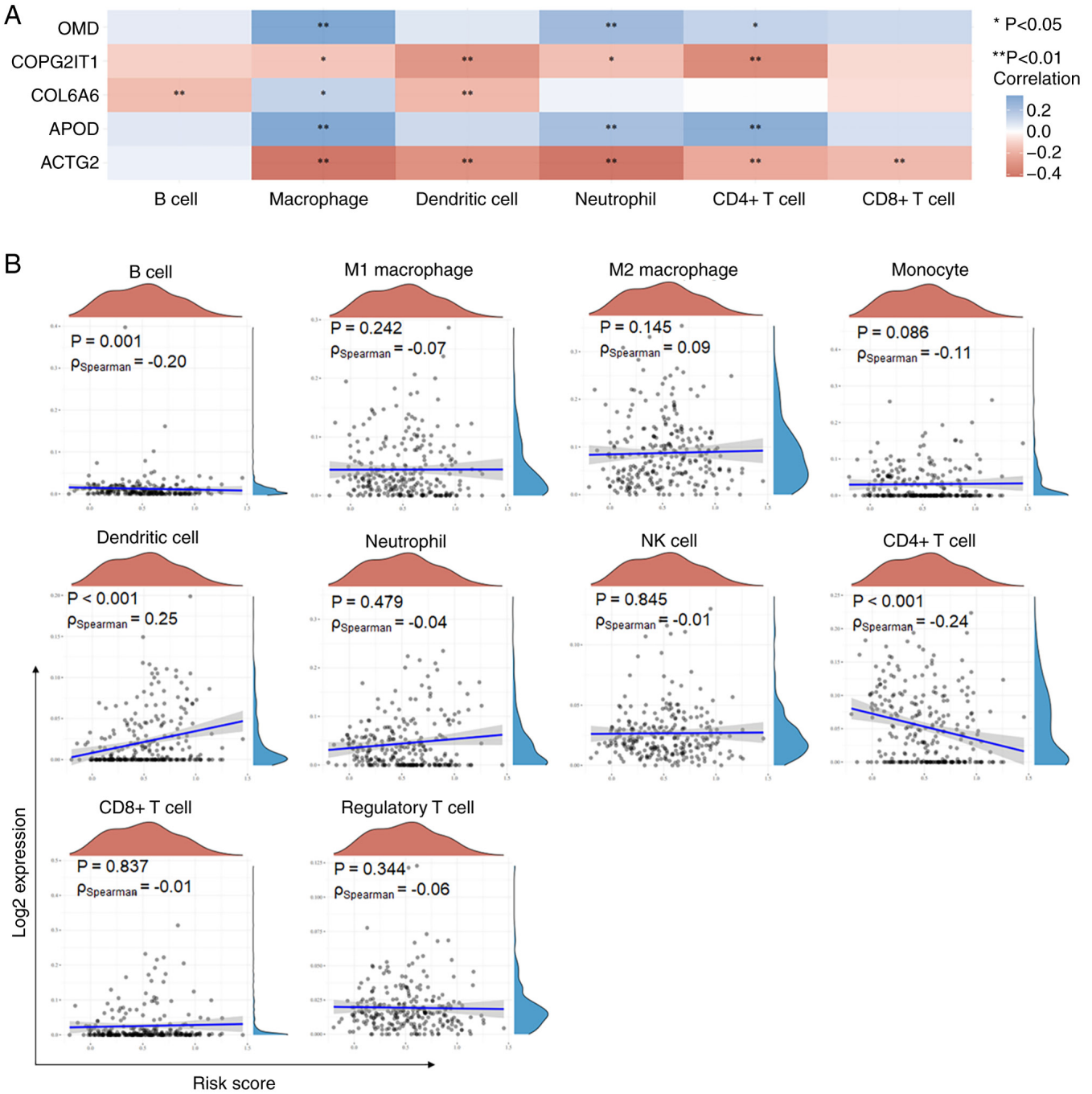

Figure 6. Immune infiltration analysis of the five gene signatures. (A) Correlation analysis comparing the five prognostic genes and six main immune cells. (B) Correlation analysis of the risk score and 10 subtypes of immune cells. *P<0.05 and **P<0.01. ACTG2, actin γ2; APOD, apolipoprotein D; COPG2IT1, coatomer protein complex subunit γ2 imprinted transcript 1; COL6A6, collagen type VI α6 chain; OMD, osteomodulin; NK, natural killer.

cell infiltration (42), thereby partially explaining the increased metastatic risk and worse prognosis in high-risk patients.

KEGG analysis revealed distinctions in the PI3K-Akt signaling pathway between the risk groups in both the GEO and TCGA datasets (P=0.0024; data not shown), although it was not in the top 10 pathways. The PI3K-Akt pathway is recognized as a critical promoter of various tumors, influencing their onset and progression (43-46). Consequently, therapies targeting the PI3K-Akt pathway have been explored in the clinical management of various cancer types, including thymomas (43), breast cancer (45), and endometrial cancer (44). The present findings suggest that the PI3K-Akt pathway is activated in the high-risk group, highlighting the potential efficacy of targeted therapies in these patients. Moreover, within the prognosis prediction model, APOD and COL6A6 were found to suppress the PI3K-Akt pathway (31,47), while activation of this pathway upregulated OMD expression (48).

With the advancement of research into tumor immunology, new technologies and methods will be increasingly applied to the staging and treatment of ASTS (3,4). Accordingly, the immune cell infiltration within tumor tissues of high- and low-risk patients were analyzed in the present study. The analysis revealed that the risk score was negatively correlated with

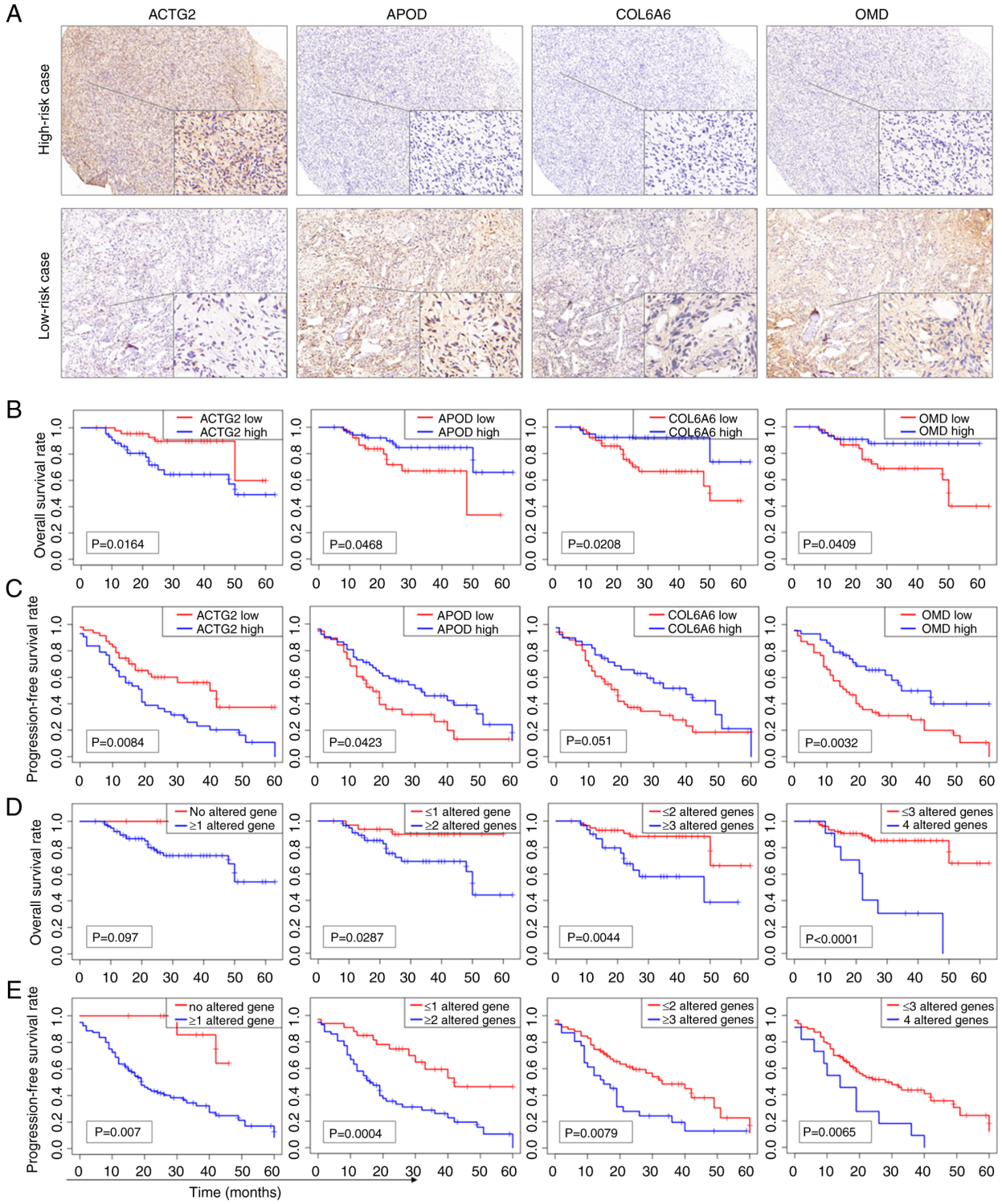

Figure 7. IHC staining analysis of prognosis-related genes in the clinical validation cohort. (A) IHC staining of a high-risk case showing high expression of ACTG2 and low expression of APOD, COL6A6 and OMD, and a low-risk case displaying low expression of ACTG2 and high expression of APOD, COL6A6 and OMD (main image, x40 magnification, and inset image, x400 magnification). (B) KM curves of OS for ACTG2, APOD, COL6A6 and OMD based on the IHC staining results. (C) KM curves of PFS for ACTG2, APOD, COL6A6 and OMD. High expression of ACTG2 and low expression of APOD, COL6A6 or OMD were considered altered genes. (D) KM curves of OS for the number of altered genes. (E) KM curves of PFS for the number of altered genes. KM, Kaplan-Meier; IHC, immunohistochemistry; ACTG2, actin γ2; APOD, apolipoprotein D; COL6A6, collagen type VI α6 chain; OMD, osteomodulin; OS, overall survival; PFS, progression-free survival.

B-cell and $CD4^+$ T-cell infiltration, and positively correlated with DC infiltration. DCs primarily serve as antigen-presenting cells (49), while B and $CD4^+$ T cells are recognized as promoters of the antitumor immune response (50). These findings highlight the complex differences in the immune microenvironment of the two risk groups.

ASTS encompasses various sarcoma subtypes, all of which have a low rate of incidence. To determine the effectiveness of

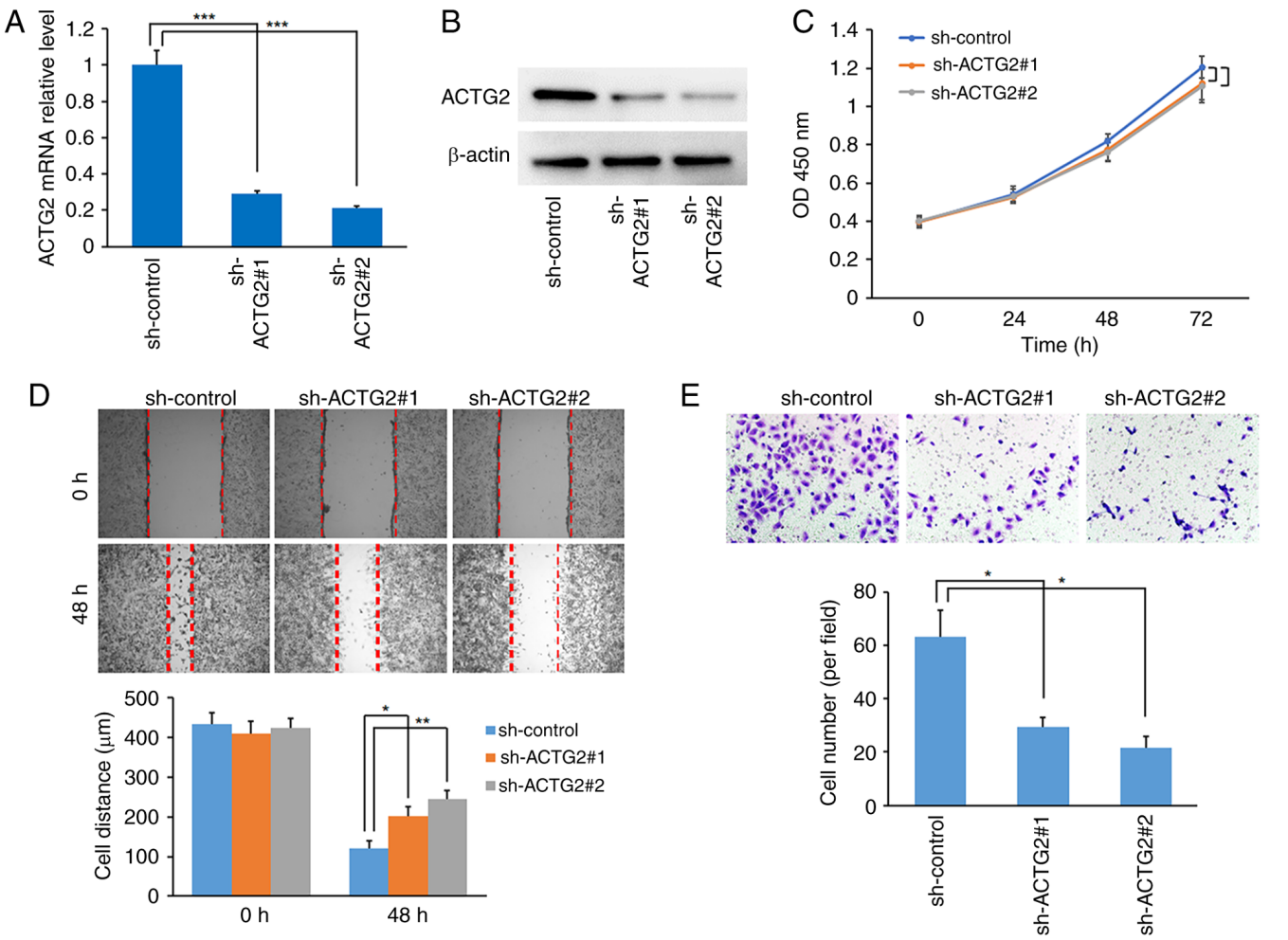

Figure 8. Inhibition of ACTG2 suppresses sarcoma cell migration and invasion. (A and B) Expression of ACTG2 in HOS cells transfected with sh-control, sh-ACTG2#1 or sh-ACTG2#2, as examined by (A) reverse transcription-quantitative PCR assay and (B) western blot assay. (C) Cell counting Kit-8 assay for HOS cells following transfection with sh-control or sh-ACTG2#1/2. (D) Evaluation of migration capacity in HOS cells post-transfection with sh-control or sh-ACTG2#1/2, using a wound healing assay (x40 magnification). (E) Assessment of invasion capacity in HOS cells post-ACTG2 knockdown, using a Transwell assay with Matrigel (x400 magnification). *P<0.05; **P<0.01; ***P<0.001. ACTG2, actin γ2; sh, short hairpin; OD, optical density.

the prognosis prediction model for a specific sarcoma subtype, the present study model was constructed based on mRNA profiles, which are often challenging to obtain from clinical patients. IHC staining is a prevalent diagnostic method in clinical settings. To assess the potential application of this model in a clinical context, 90 osteosarcoma samples were collected and the expression of genes from the prognosis prediction model were analyzed through IHC staining. It was found that low expression levels of ACTG2, but high expression levels of APOD, COL6A6 and OMD, were all associated with a favorable patient prognosis. Furthermore, the combination of multiple altered genes provided a more distinct differentiation between OS and PFS than any single gene. These findings suggest that leveraging multiple genes in the prognosis prediction model can improve prognosis accuracy for patients with ASTS.

The present study is not without limitations. First, the stage of ASTS is not available in both the GEO and TCGA datasets, restricting the analysis of the correlation between the prognosis prediction model and the clinical stages of ASTS. Second, a direct link between the risk score and immunization activity has not yet been established. Third, although the model was validated in a single sarcoma subtype using IHC staining, conducting RT-qPCR assays in more ASTS subtypes and with a larger patient cohort could better assess the clinical applicability of the prognostic model. Fourth, there is a crossing phenomenon at the beginning or the end of some survival curves, which may have a certain impact on the statistical results. However, at present, there is no universally recognized and mature method to resolve this issue (51). Lastly, the potential roles of the other four genes in ASTS warrant further investigation in future studies.

In conclusion, in the present study, a prognosis prediction model for ASTS was developed by analyzing DEGs in patients with metastatic cancer, which was then validated in external patient cohorts. Functional and pathway analyses identified significant differences in stemness, ECM and cell adhesion-related pathways between the two risk groups, underscoring the importance of PI3K-Akt pathway activation in high-risk cases. Changes in immune cell infiltration were also correlated with the risk score. This metastasis-based prediction model not only serves as a valuable tool for predicting the survival of patients with ASTS, but also establishes a foundation for future investigations into the process of tumor metastasis.

Acknowledgements

Not applicable.

Funding

This research was funded by the National Natural Science Youth Fund (grant no. 82003132), the Long Voyage Plan of Shanghai Pudong New Area People's Hospital (grant no. PRYYH202301), the Excellent Young Medical Talents Training Program at the Shanghai Pudong New Area People's Hospital (grant no. PWRq2021-33) and the Project of Clinical Outstanding Clinical Discipline Construction in Shanghai Pudong New Area (grant no. PWYgy2021-08).

Availability of data and materials

The data generated in the present study may be requested from the corresponding author.

Authors' contributions

SH, JT and JW conceptualized and designed the study. SH and XS performed the data analyses. SH and JT interpreted the results. JL and JZ collected the clinical samples. ZW and HS conducted the IHC staining. SH and JT performed the *in vitro* studies. XS and JT drafted the manuscript, which was revised by JT. SH and XS confirm the authenticity of all the raw data. All authors have read and approved the final manuscript.

Ethics approval and consent to participate

This study was reviewed and approved by the Medical Ethics Committees of Shanghai Changzheng Hospital (Shanghai, China; approval no. 2018SL004) and Shanghai Pudong New Area People's Hospital (Shanghai, China; approval no. K82 of 2021). Written informed consent was obtained from all participating patients or their legal guardians.

Patient consent for publication

Written informed consent for publication was obtained from all individuals involved in the study.

Competing interests

The authors declare that they have no competing interests.

References

1. Li Z, Duan Z, Jia K, Yao Y, Liu K, Qiao Y, Gao Q, Yang Y, Li G and Shang A: A combined risk score model to assess prognostic value in patients with soft tissue sarcomas. Cells 11: 4077, 2022.
2. Siegel RL, Miller KD and Jemal A: Cancer statistics, 2018. CA Cancer J Clin 68: 7-30, 2018.
3. Gamboa AC, Gronchi A and Cardona K: Soft-tissue sarcoma in adults: An update on the current state of histiotype-specific management in an era of personalized medicine. CA Cancer J Clin 70: 200-229, 2020.
4. Ardakani AHG, Woollard A, Ware H and Gikas P: Soft tissue sarcoma: Recognizing a rare disease. Cleve Clin J Med 89: 73-80, 2022.
5. Chen HH, Zhang TN, Zhang FY and Zhang T: Non-coding RNAs in drug and radiation resistance of bone and soft-tissue sarcoma: A systematic review. Elife 11: e79655, 2022.
6. Xu R, Qi L, Ren X, Zhang W, Li C, Liu Z, Tu C and Li Z: Integrated analysis of TME and hypoxia identifies a classifier to predict prognosis and therapeutic biomarkers in soft tissue sarcomas. Cancers (Basel) 14: 5675, 2022.
7. Gu HY, Lin LL, Zhang C, Yang M, Zhong HC and Wei RX: The potential of five immune-related prognostic genes to predict survival and response to immune checkpoint inhibitors for soft tissue sarcomas based on multi-omic study. Front Oncol 10: 1317, 2020.
8. Chibon F, Lagarde P, Salas S, Pérot G, Brouste V, Tirode F, Lucchesi C, de Reynies A, Kauffmann A, Bui B, *et al*: Validated prediction of clinical outcome in sarcomas and multiple types of cancer on the basis of a gene expression signature related to genome complexity. Nat Med 16: 781-787, 2010.
9. Proost JH and Eleveld DJ: Performance of an iterative two-stage bayesian technique for population pharmacokinetic analysis of rich data sets. Pharm Res 23: 2748-2759, 2006.
10. Livak KJ and Schmittgen TD: Analysis of relative gene expression data using real-time quantitative PCR and the 2(-Delta Delta C(T)) method. Methods 25: 402-408, 2001.
11. Zhang H, Wang T, Gong HY, Jiang RY, Zhou W, Sun HT, Huang R, Wang Y, Wu Z, Xu W, *et al*: A novel molecular classification method for osteosarcoma based on tumor cell differentiation trajectories. Bone Res 11: 1, 2023.
12. Lepucki A, Orlińska K, Mielczarek-Palacz A, Kabut J, Olczyk P and Komosińska-Vassev K: The role of extracellular matrix proteins in breast cancer. J Clin Med 11: 1250, 2022.
13. Song Y, Ma X, Zhang M, Wang M, Wang G, Ye Y and Xia W: Ezrin mediates invasion and metastasis in tumorigenesis: A review. Front Cell Dev Biol 8: 588801, 2020.
14. Rømer AMA, Thorseth ML and Madsen DH: Immune modulatory properties of collagen in cancer. Front Immunol 12: 791453, 2021.
15. Yan JY, Gong HY, Han S, Liu JL, Wu ZP, Wang ZH and Wang T: GALNT5 functions as a suppressor of ferroptosis and a predictor of poor prognosis in pancreatic adenocarcinoma. Am J Cancer Res 13: 4579-4596, 2023.
16. Crombé A, Roulleau-Dugage M and Italiano A: The diagnosis, classification, and treatment of sarcoma in this era of artificial intelligence and immunotherapy. Cancer Commun (Lond) 42: 1288-1313, 2022.
17. Lynch MM, Alexiev BA, Schroeder BA and Pollack SM: Combinations of chemotherapy and PD-1/PD-L1 inhibitors in sarcoma. Curr Treat Options Oncol 23: 1861-1876, 2022.
18. Milunsky A, Baldwin C, Zhang X, Primack D, Curnow A and Milunsky J: Diagnosis of chronic intestinal pseudo-obstruction and megacystis by sequencing the ACTG2 gene. J Pediatr Gastroenterol Nutr 65: 384-387, 2017.
19. Zhao B, Baloch Z, Ma Y, Wan Z, Huo Y, Li F and Zhao Y: Identification of potential key genes and pathways in early-onset colorectal cancer through bioinformatics analysis. Cancer Control 26: 1073274819831260, 2019.
20. Tang G, Wu D, Guo M and Li H: LncRNA MIR497HG inhibits colorectal cancer progression by the miR-3918/ACTG2 axis. J Genet 101: 27, 2022.
21. Wu Y, Liu ZG, Shi MQ, Yu HZ, Jiang XY, Yang AH, Fu XS, Xu Y, Yang S, Ni H, *et al*: Identification of ACTG2 functions as a promoter gene in hepatocellular carcinoma cells migration and tumor metastasis. Biochem Biophys Res Commun 491: 537-544, 2017.
22. Davis LE, Nusser KD, Przybyl J, Pittsenbarger J, Hofmann NE, Varma S, Vennam S, Debiec-Rychter M, van de Rijn M and Davare MA: Discovery and characterization of recurrent, targetable ALK fusions in leiomyosarcoma. Mol Cancer Res 17: 676-685, 2019.
23. Beck AH, Lee CH, Witten DM, Gleason BC, Edris B, Espinosa I, Zhu S, Li R, Montgomery KD, Marinelli RJ, *et al*: Discovery of molecular subtypes in leiomyosarcoma through integrative molecular profiling. Oncogene 29: 845-854, 2010.
24. Jankovic-Karasoulos T, Bianco-Miotto T, Butler MS, Butler LM, McNeil CM, O'Toole SA, Millar EKA, Sakko AJ, Ruiz AI, Birrell SN, *et al*: Elevated levels of tumour apolipoprotein D independently predict poor outcome in breast cancer patients. Histopathology 76: 976-987, 2020.
25. Zhang Y, Qin Y, Li D and Yang Y: A risk prediction model mediated by genes of APOD/APOC1/SQLE associates with prognosis in cervical cancer. BMC Womens Health 22: 534, 2022.

26. Ruchong P, Haiping T and Xiang W: A five-gene prognostic nomogram predicting disease-free survival of differentiated thyroid cancer. Dis Markers 2021: 5510780, 2021.
27. Palmerini E, Gambarotti M, Staals EL, Zanella L, Sieberova G, Longhi A, Cesari M, Bonarelli S, Picci P, Ruggieri P, *et al*: Fibrosarcomatous changes and expression of CD34+ and apolipoprotein-D in dermatofibrosarcoma protuberans. Clin Sarcoma Res 2: 4, 2012.
28. Green BB, Kappil M, Lambertini L, Armstrong DA, Guerin DJ, Sharp AJ, Lester BM, Chen J and Marsit CJ: Expression of imprinted genes in placenta is associated with infant neurobehavioral development. Epigenetics 10: 834-841, 2015.
29. Mai X, Mai Q, Li T and Zhou C: Dynamic expression patterns of imprinted genes in human embryonic stem cells following prolonged passaging and differentiation. J Assist Reprod Genet 28: 315-323, 2011.
30. Kang SH, Oh SY, Lee HJ, Kwon TG, Kim JW, Lee ST, Choi SY and Hong SH: Cancer-associated fibroblast subgroups showing differential promoting effect on HNSCC progression. Cancers (Basel) 13: 654, 2021.
31. Long R, Liu Z, Li J and Yu H: COL6A6 interacted with P4HA3 to suppress the growth and metastasis of pituitary adenoma via blocking PI3K-Akt pathway. Aging (Albany NY) 11: 8845-8859, 2019.
32. Qiao H, Feng Y and Tang H: COL6A6 inhibits the proliferation and metastasis of non-small cell lung cancer through the JAK signalling pathway. Transl Cancer Res 10: 4514-4522, 2021.
33. Ma Y, Qiu M, Guo H, Chen H, Li J, Li X and Yang F: Comprehensive analysis of the immune and prognostic implication of COL6A6 in lung adenocarcinoma. Front Oncol 11: 633420, 2021.
34. Skenteris NT, Seime T, Witasp A, Karlöf E, Wasilewski GB, Heuschkel MA, Jaminon AMG, Oduor L, Dzhanaev R, Kronqvist M, *et al*: Osteomodulin attenuates smooth muscle cell osteogenic transition in vascular calcification. Clin Transl Med 12: e682, 2022.
35. Hamaya E, Fujisawa T and Tamura M: Osteoadherin serves roles in the regulation of apoptosis and growth in MC3T3-E1 osteoblast cells. Int J Mol Med 44: 2336-2344, 2019.
36. Papadaki V, Asada K, Watson JK, Tamura T, Leung A, Hopkins J, Dellett M, Sasai N, Davaapil H, Nik-Zainal S, *et al*: Two secreted proteoglycans, activators of urothelial cell-cell adhesion, negatively contribute to bladder cancer initiation and progression. Cancers (Basel) 12: 3362, 2020.
37. Nallasamy P, Nimmakayala RK, Parte S, Are AC, Batra SK and Ponnusamy MP: Tumor microenvironment enriches the stemness features: The architectural event of therapy resistance and metastasis. Mol Cancer 21: 225, 2022.
38. Rodrigues FS, Ciccarelli FD and Malanchi I: Reflected stemness as a potential driver of the tumour microenvironment. Trends Cell Biol 32: 979-987, 2022.
39. Gao Y, Fan WH, Song Z, Lou H and Kang X: Comparison of circulating tumor cell (CTC) detection rates with epithelial cell adhesion molecule (EpCAM) and cell surface vimentin (CSV) antibodies in different solid tumors: A retrospective study. PeerJ 9: e10777, 2021.
40. Ventura E, Xie C, Buraschi S, Belfiore A, Iozzo RV, Giordano A and Morrione A: Complexity of progranulin mechanisms of action in mesothelioma. J Exp Clin Cancer Res 41: 333, 2022.
41. Fromme JE and Zigrino P: The role of extracellular matrix remodeling in skin tumor progression and therapeutic resistance. Front Mol Biosci 9: 864302, 2022.
42. Kolesnikoff N, Chen CH and Samuel MS: Interrelationships between the extracellular matrix and the immune microenvironment that govern epithelial tumour progression. Clin Sci (Lond) 136: 361-377, 2022.
43. Abu Zaid MI, Radovich M, Althouse S, Liu H, Spittler AJ, Solzak J, Badve S and Loehrer PJ Sr: A phase II study of buparlisib in relapsed or refractory thymomas. Front Oncol 12: 891383, 2022.
44. Heudel P, Frenel JS, Dalban C, Bazan F, Joly F, Arnaud A, Abdeddaim C, Chevalier-Place A, Augereau P, Pautier P, *et al*: Safety and efficacy of the mTOR inhibitor, vistusertib, combined with anastrozole in patients with hormone receptor-positive recurrent or metastatic endometrial cancer: The VICTORIA multicenter, open-label, phase 1/2 randomized clinical trial. JAMA Oncol 8: 1001-1009, 2022.
45. Savas P, Lo LL, Luen SJ, Blackley EF, Callahan J, Moodie K, van Geelen CT, Ko YA, Weng CF, Wein L, *et al*: Alpelisib monotherapy for PI3K-altered, pretreated advanced breast cancer: A phase II study. Cancer Discov 12: 2058-2073, 2022.
46. Xu C, Wang Z, Zhang L, Feng Y, Lv J, Wu Z, Yang R, Wu T, Li J, Zhou R, *et al*: Periostin promotes the proliferation and metastasis of osteosarcoma by increasing cell survival and activates the PI3K/Akt pathway. Cancer Cell Int 22: 34, 2022.
47. Yu RH, Zhang XY, Xu W, Li ZK and Zhu XD: Apolipoprotein D alleviates glucocorticoid-induced osteogenesis suppression in bone marrow mesenchymal stem cells via the PI3K/Akt pathway. J Orthop Surg Res 15: 307, 2020.
48. Guntur AR, Rosen CJ and Naski MC: N-cadherin adherens junctions mediate osteogenesis through PI3K signaling. Bone 50: 54-62, 2012.
49. Patente TA, Pinho MP, Oliveira AA, Evangelista GCM, Bergami-Santos PC and Barbuto JAM: Human dendritic cells: Their heterogeneity and clinical application potential in cancer immunotherapy. Front Immunol 9: 3176, 2019.
50. Liu D, Heij LR, Czigany Z, Dahl E, Lang SA, Ulmer TF, Luedde T, Neumann UP and Bednarsch J: The role of tumor-infiltrating lymphocytes in cholangiocarcinoma. J Exp Clin Cancer Res 41: 127, 2022.
51. Li H, Han D, Hou Y, Chen H and Chen Z: Statistical inference methods for two crossing survival curves: A comparison of methods. PLoS One 10: e0116774, 2015.